Journal of Magnetic Resonance **145,** 230–236 (2000)
doi:10.1006/jmre.2000.2084, available online at http://www.idealibrary.com on IDEAL®

A High-Resolution ^{13}C 3D CSA-CSA-CSA Correlation Experiment by Means of Magic Angle Turning

Jian Zhi Hu,* Chaohui Ye,† Ronald J. Pugmire,‡ and David M. Grant*

**Department of Chemistry and ‡Department of Chemical and Fuels Engineering, University of Utah, Salt Lake City, Utah 84112; and †The State Key Laboratory of NMR and Atomic and Molecular Physics, Wuhan Institute of Physics, The Chinese Academy of Sciences, China*

Received November 1, 1999; revised March 2, 2000

It is shown in this paper that a previously reported 90° sample flipping ^{13}C 2D CSA-CSA correlation experiment may be carried out alternatively by employing constant slow sample rotation about the magic angle axis and by synchronizing the read pulse to $\frac{1}{3}$ of the rotor cycle. A high-resolution 3D CSA-CSA-CSA correlation experiment based on the magic angle turning technique is reported in which the conventional 90° 2D CSA-CSA powder pattern for each carbon in a system containing a number of inequivalent carbons may be separated according to the isotropic chemical shift value. The technique is demonstrated on 1,2,3-trimethoxybenzene in which all of the overlapping powder patterns that cannot be segregated by the 2D CSA-CSA experiment are resolved successfully by the 3D CSA-CSA-CSA experiment, including even the two methoxy groups (M_1 and M_3) whose isotropic shifts, confirmed by high-speed MAS, are separated by only 1 ppm. A difference of 4 ppm in the principal value component (δ_{33}) between M_1 and M_3 is readily obtained.

Key Words: **solid state NMR; magic angle turning (MAT); chemical shift anisotropy (CSA); 2D CSA-CSA correlation; 3D CSA-CSA-CSA correlation.**

1. INTRODUCTION

The two-dimensional magic angle turning (2D MAT) experiment first reported by Gan (*1*) has been developed into a powerful tool for the measurement of the principal values of chemical shift tensors in powdered solids with complex molecular structure (*2–10*). Based on the magic angle hopping experiment (*11, 12*) initially reported by Bax *et al.* (*11*), the MAT experiment is easier to perform for a number of reasons. First, the magic angle can be set experimentally with high accuracy. Second, the read pulses may be spaced accurately at $\frac{1}{3}$ of the rotor cycle with the aid of a simple rotor synchronization device (*4*). Third, the experiment may be carried out using either simple homemade large-sample-volume probes (*3, 4*) or commercially available MAS probes (*1, 5, 6*). Because of the very slow sample spinning employed in the MAT experiment, a large sample volume can be used that provides high sensitivity for the measurement.

The MAT experiment has been extended to produce a number of new and useful multidimension solid-state NMR experiments. These modifications allow important interactions to be isolated in experiments with additional dimensions. The concept has been successfully demonstrated recently with the development of a high-resolution 3D separated-local-field experiment (*13*).

It has been shown that a 2D CSA-CSA correlation spectrum is useful for extracting CSA principal values in powdered solids (*14*) and it is especially attractive for obtaining the orientation parameters of molecules in an oriented sample (*15–17*). The 2D CSA-CSA correlation experiment, based on earlier work by Henrichs (*18*), was developed by the Grant (*14, 15*) and Spiess (*16, 17*) groups, especially for polymer samples. A 90° (*14, 15*) or a 45° (*16, 17*) sample reorientation is generally used in this type of experiment. The sample reorientation has been achieved mechanically using a reorientational flipping mechanism, in which the sample is quickly rotated 90 or 45° about an axis perpendicular to the magnetic field direction. Since a 90° or a 45° sample reorientation about the magnetic field can be alternatively realized by rotating the sample 120° or 55.9° about an axis inclined at the magic angle, these sample reorientations may be carried out in a magic angle turning experiment. In the process, one creates a MAT 2D CSA-CSA sequence.

A limitation of the reorientational 2D CSA-CSA correlation spectrum is the broad powder patterns from different types of carbons that are superimposed and are often indistinguishable from one another when there are a number of inequivalent carbons in the sample. In order to identify the individual powder pattern for each inequivalent carbon in a complex system, a 3D experiment generally should be employed. In this work, a high-resolution 3D CSA-CSA-CSA experiment based on the MAT technique is reported, in which the conventional 90° 2D CSA-CSA powder pattern for each carbon may be segregated by its isotropic chemical shift value. The 3D CSA-CSA-CSA experiment presented in this paper is an alternative to the slow-spinning version of the 3D DECODER experiment (essentially an isotropic-CSA-CSA 3D correlation experiment) introduced previously by Lewis *et al.* (*19*). The isotropic dimension was produced by Gan's original MAT sequence as an independent dimension.

1090-7807/00 $35.00

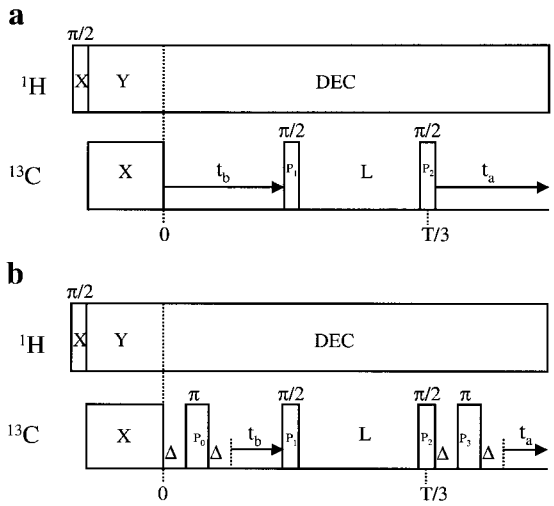

FIG. 1. The pulse sequence for the ^{13}C MAT 2D CSA-CSA correlation experiment. During the time period labeled "*L*," the magnetization is stored along the magnetic field direction by the 90° projection pulse labeled P_1. "*T*" is the rotor period. The phase cycling for the pulses are generated based on those given in Ref. (*14*) by adding phase cycling for the π pulses. (a). The model MAT pulse sequence. (b). The echo-MAT CSA-CSA sequence.

2. THEORY

2.1. The ^{13}C MAT 2D CSA-CSA Correlation Experiment

The pulse sequence for the MAT 90° CSA-CSA correlation experiment is shown in Fig. 1a. The slow sample turning period is constant and denoted by *T*. The ^{13}C transverse magnetization is created by the conventional cross-polarization method. At the end of the evolution time t_b, a 90° projection pulse labeled P_1 stores either the cosine or the sine component of the magnetization along the longitudinal field direction. The transverse magnetization component decays by transverse relaxation during the store period labeled *L*. The 90° read pulse, labeled P_2, is synchronized to $\frac{1}{3}$ of the rotor cycle relative to the end of the cross-polarization pulse. By phase cycling the projection pulse P_1, the hypercomplex (*20*) FID is

$$F(t_a, t_b) = M_0 \exp(j\phi_b(t_b) - t_b/T_2)\exp(i\phi_a(t_a) - t_a/T_2), \quad [1]$$

where $\exp(j\phi_b(t_b) - t_b/T_2)$ or $\exp(i\phi_a(t_a) - t_a/T_2)$ represents the time dependence of the FID obtained from a rotating sample. This FID produces a spinning-sideband spectrum whose features depend on the principal values of the chemical shift tensor and decay in the usual way with the time constant T_2. Since the initial sample positions for dimension (a) and dimension (b) are perpendicular in space, Eq. [1] represents a 2D FID for a rotating sample that correlates two initially orthogonal magnetic field directions. When a slow sample rotation rate, e.g., 20–50 Hz, is used, the spinning sidebands are no longer distinguishable from one another and the overlapping sideband spectrum approaches that of a stationary sample. An essentially identical 2D powder pattern may be obtained by using either the conventional "flipper" technique (*14*) or this MAT method.

The dead time, inherent with the pulse sequence in Fig. 1a, may be eliminated with a symmetric double echo sequence depicted in Fig. 1b. The FID obtained by this modified pulse sequence is

$$\begin{aligned} F(t_a, t_b) &= M_0 \exp[j(\Psi_b + \phi_b) - (t_b + 2\Delta)/T_2] \\ &\quad \times \exp[i(\Psi_a + \phi_a) - (t_a + 2\Delta)/T_2] \\ &= \mathbf{K} \cdot \mathrm{FID}(t_a, t_b), \end{aligned} \quad [2]$$

where

$$\mathbf{K} = \exp(j\Psi_b)\exp(i\Psi_a), \quad [3]$$

$$\begin{aligned} \mathrm{FID}(t_a, t_b) &= M_0 \exp[j\phi_b(t_b) - (t_b + 2\Delta)/T_2] \\ &\quad \times \exp[i\phi_a(t_a) - (t_a + 2\Delta)/T_2]. \end{aligned} \quad [4]$$

In general, the phase angles, Ψ_a and Ψ_b, will be different for different crystal orientations in a rotating sample (*21*) and cannot be eliminated through phase corrections. Fortunately, at a very slow turning rate, **K** approaches 1 and the phase distortion becomes negligible. The spectrum produced by the pulse sequence in Fig. 1b resembles the conventional CSA-CSA correlation spectrum.

2.2. The ^{13}C MAT 3D CSA-CSA-CSA Correlation Experiment

The generalization of a 3D CSA-CSA-CSA correlation spectrum is best illustrated with the simplest model pulse sequence shown in Fig. 2a. The read pulses are labeled with phases *Y* and *X* in the ^{13}C channel and are synchronized to $\frac{1}{3}$ of the rotor cycle. In this way, the orientations of the sample are mutually perpendicular initially with respect to each other during the acquisition (a), evolution (b), and evolution (c) dimensions, respectively. The acquired 3D hypercomplex data sets, which are obtained by phase cycling the projection pulses P_1 and P_2, are as follows:

$$\begin{aligned} &F_1(t_c, t_b, t_a) \\ &\quad = \cos(\phi(t_c))\cos(\phi(t_b))\, F_a(t_a)\exp(-(t_c + t_b)/T_2) \end{aligned} \quad [5]$$

$$\begin{aligned} &F_2(t_c, t_b, t_a) \\ &\quad = \cos(\phi(t_c))\sin(\phi(t_b))\, F_a(t_a)\exp(-(t_c + t_b)/T_2) \end{aligned} \quad [6]$$

$$\begin{aligned} &F_3(t_c, t_b, t_a) \\ &\quad = \sin(\phi(t_c))\cos(\phi(t_b))\, F_a(t_a)\exp(-(t_c + t_b)/T_2) \end{aligned} \quad [7]$$

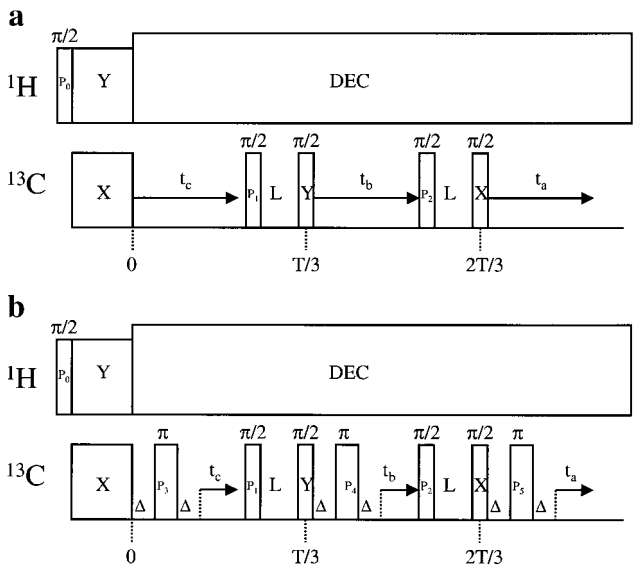

FIG. 2. The pulse sequences for the high-resolution MAT 3D CSA-CSA-CSA experiment. The t_b and t_c are the second and the third evolution periods and Δ is the echo delay used to avoid probe ring-down and receiver recovery. (a). The model pulse sequence for the MAT 3D CSA-CSA-CSA experiment. (b). The echo pulse sequence for the MAT 3D CSA-CSA-CSA experiment.

$$F_4(t_c, t_b, t_a) = \sin(\phi(t_c))\sin(\phi(t_b))\,F_a(t_a)\exp(-(t_c + t_b)/T_2). \quad [8]$$

The four sets of hypercomplex data are then collected in the following way to obtain the sine and cosine components of the magnetization for the evolution (c) dimension:

$$\begin{aligned} F_c(t_c, t_b, t_a) &= F_1(t_c, t_b, t_a) + jF_2(t_c, t_b, t_a) \\ &= \cos(\phi(t_c))\exp(j\phi(t_b))\,F_a(t_a)\exp(-(t_c + t_b)/T_2) \\ &= \cos(\phi(t_c))\,F_b(t_b)\,F_a(t_a)\exp(-t_c/T_2), \end{aligned} \quad [9]$$

$$\begin{aligned} F_s(t_c, t_b, t_a) &= F_3(t_c, t_b, t_a) + jF_4(t_c, t_b, t_a) \\ &= \sin(\phi(t_c))\exp(j\phi(t_b))\,F_a(t_a)\exp(-(t_c + t_b)/T_2) \\ &= \sin(\phi(t_c))\,F_b(t_b)\,F_a(t_a)\exp(-t_c/T_2). \end{aligned} \quad [10]$$

One obtains

$$\begin{aligned} F(t_c, t_b, t_a) &= F_c(t_c, t_b, t_a) + kF_s(t_c, t_b, t_a) \\ &= F_c(t_c)\,F_b(t_b)\,F_a(t_a), \end{aligned} \quad [11]$$

where, $F_a(t_a) = M_0\exp(i\phi(t_a) - t_a/T_2)$, $F_b(t_b) = \exp(j\phi(t_b) - t_b/T_2)$, and $F_c(t_c) = \exp(k\phi(t_c) - t_c/T_2)$ are the FIDs for the acquisition (a), evolution (b), and evolution (c), respectively. Each of these FIDs may be identified with one of the orthogonal axes associated with the different principal values of the chemical shift tensor. The time constants, T_2, of these FIDs are assumed to be isotropic in character. Since the initial sample orientations for dimensions a, b, and c are mutually perpendicular in space, Eq. [11] represents a 3D hypercomplex FID of a slowly rotating sample which correlates three mutually perpendicular magnetic field directions. At a slow turning rate, e.g., 20–50 Hz, the numerous spinning sidebands merge together. The powder pattern of a slowly rotating sample approaches that which would be obtained from a stationary sample. The Fourier transformation of Eq. [11] gives a 3D spectrum, in which the powder pattern for each carbon is separated into planes (isotropic shift planes) perpendicular to the body diagonal of the cubic spectrum. The 1D projection of the cubic spectrum onto its diagonal resembles the 1D MAS spectrum. A 2D projection onto any one of the cube faces (i.e., F_a–F_b, F_a–F_c, and F_b–F_c) is a typical 2D CSA-CSA correlation spectrum. A selected projection of an isotropic shift plane for a specific carbon to the F_a–F_b 2D spectral plane produces the familiar 2D CSA-CSA spectrum for the corresponding carbon.

A disadvantage of the model 3D pulse sequence in Fig. 2a arises from the poor quality of the 3D spectrum due to the dead time associated with probe ring-down and receiver recovery. A symmetric triple-echo sequence is incorporated to suppress these dead time distortions and the resultant pulse sequence is given in Fig. 2b. The phase cycling for the pulses in Fig. 2b is summarized in Table 1. Hypercomplex data are acquired and collected in the same way as described for the pulse sequence in Fig. 2a. The result is described by Eq. [12]:

$$F(t_c, t_b, t_a) = \mathbf{K}F_c(t_c)\,F_b(t_b)\,F_a(t_a)\exp(-6\Delta/T_2), \quad [12]$$

where

$$\begin{aligned} \mathbf{K} &= \exp(k\Psi_c)\exp(j\Psi_b)\exp(i\Psi_a) \\ F_a(t_a) &= M_0\exp(i\phi(t_a) - t_a/T_2), \\ F_b(t_b) &= \exp(j\phi(t_b) - t_b/T_2), \\ F_c(t_c) &= \exp(k\phi(t_c) - t_c/T_2). \end{aligned} \quad [13]$$

Although $\Psi_c + \Psi_b + \Psi_a = 0$ is satisfied for a rotating sample because the triple-echo sequence is equally spaced around the circle (*3*), the three phases, Ψ_a, Ψ_b, and Ψ_c, in Eq. [13] cannot be added together as i, j, and k are three independent complex components. This triple-echo sequence in Fig. 2b produces a perfect chemical shift echo only at the limit of the zero rotating frequency, or alternatively, as Δ/T approaches zero. This feature is described in Ref. (*3*) for the triple-echo MAT experiment. At very slow sample rotation, **K** approaches unity.

TABLE 1
The Phase Table for the High-Resolution MAT 3D CSA-CSA-CSA Correlation Experiment

Pulse	1	2	3	4	5	6	7	8	Magnetization
P_0	$+X$	$+X$	$+X$	$+X$	$-X$	$-X$	$-X$	$-X$	
P_1	$+Y$	$+Y$	$-Y$	$-Y$	$+Y$	$+Y$	$-Y$	$-Y$	
P_2	$+Y$	$-Y$	$+Y$	$-Y$	$+Y$	$-Y$	$+Y$	$-Y$	
P_3	$+X$	$+X$	$+X$	$+X$	$+X$	$+X$	$+X$	$+X$	
P_4	$+X$	$+X$	$+X$	$+X$	$+X$	$+X$	$+X$	$+X$	
P_5	$+Y$	$+Y$	$+Y$	$+Y$	$+Y$	$+Y$	$+Y$	$+Y$	
Receiver	$+Y$	$-Y$	$-Y$	$+Y$	$-Y$	$+Y$	$+Y$	$-Y$	$F_1(t_c, t_b, t_a)$
P_0	$+X$	$+X$	$+X$	$+X$	$-X$	$-X$	$-X$	$-X$	
P_1	$+Y$	$+Y$	$-Y$	$-Y$	$+Y$	$+Y$	$-Y$	$-Y$	
P_2	$+X$	$-X$	$+X$	$-X$	$+X$	$-X$	$+X$	$-X$	
P_3	$+X$	$+X$	$+X$	$+X$	$+X$	$+X$	$+X$	$+X$	
P_4	$+X$	$+X$	$+X$	$+X$	$+X$	$+X$	$+X$	$+X$	
P_5	$+Y$	$+Y$	$+Y$	$+Y$	$+Y$	$+Y$	$+Y$	$+Y$	
Receiver	$+Y$	$-Y$	$-Y$	$+Y$	$-Y$	$+Y$	$+Y$	$-Y$	$F_2(t_c, t_b, t_a)$
P_0	$+X$	$+X$	$+X$	$+X$	$-X$	$-X$	$-X$	$-X$	
P_1	$+X$	$+X$	$-X$	$-X$	$+X$	$+X$	$-X$	$-X$	
P_2	$+Y$	$-Y$	$+Y$	$-Y$	$+Y$	$-Y$	$+Y$	$-Y$	
P_3	$-X$	$-X$	$-X$	$-X$	$-X$	$-X$	$-X$	$-X$	
P_4	$-X$	$-X$	$-X$	$-X$	$-X$	$-X$	$-X$	$-X$	
P_5	$-Y$	$-Y$	$-Y$	$-Y$	$-Y$	$-Y$	$-Y$	$-Y$	
Receiver	$+Y$	$-Y$	$-Y$	$+Y$	$-Y$	$+Y$	$+Y$	$-Y$	$F_3(t_c, t_b, t_a)$
P_0	$+X$	$+X$	$+X$	$+X$	$-X$	$-X$	$-X$	$-X$	
P_1	$+X$	$+X$	$-X$	$-X$	$+X$	$+X$	$-X$	$-X$	
P_2	$+X$	$-X$	$+X$	$-X$	$+X$	$-X$	$+X$	$-X$	
P_3	$-X$	$-X$	$-X$	$-X$	$-X$	$-X$	$-X$	$-X$	
P_4	$-X$	$-X$	$-X$	$-X$	$-X$	$-X$	$-X$	$-X$	
P_5	$-Y$	$-Y$	$-Y$	$-Y$	$-Y$	$-Y$	$-Y$	$-Y$	
Receiver	$+Y$	$-Y$	$-Y$	$+Y$	$-Y$	$+Y$	$+Y$	$-Y$	$F_4(t_c, t_b, t_a)$

3. EXPERIMENTAL RESULTS AND DISCUSSIONS

The sample 1,2,3-trimethoxybenzene (1,2,3-TMB) was obtained from Aldrich and was used without further purification.

All of the experiments were performed on a VXR-200 NMR spectrometer with a ^{13}C frequency of 50.309 MHz. A homemade large-sample-volume MAT probe (*3*) was used to hold a 5-g sample. The power levels for the decoupling channel were 230 W for cross-polarization and about 600 W for decoupling to give, respectively, a 30-kHz field for cross-polarization and a 48-kHz field for decoupling. All data were processed with software, developed in this laboratory, running on a VAX data station.

In Fig. 3a, the MAT 2D CSA-CSA spectrum of 1,2,3-TMB is acquired using the pulse sequence in Fig. 1b at a sample turning rate of 44 $\pm$ 0.2 Hz. This spectrum was acquired with the following experimental conditions. The spectral widths are $sw_a = sw_b = 20{,}000$ Hz, corresponding to a time increment of 50 μs for both dimensions. A contact time of 4 ms and a Δ value of 60 μs were used. Hypercomplex data sets were acquired with 64 t_b increments in the evolution dimension; 64 scans with a recycle delay time of 8 s were acquired for both the real and the imaginary FIDs at each t_b increment. The total measurement time was about 20 h.

Three conventional 90° sample reorientation 2D CSA-CSA patterns (*14*) are easily recognized in Fig. 3a, indicating that the replacement of the rapid mechanical reorientation with constant slow sample turning is practical. The ^{13}C MAT 2D CSA-CSA spectrum may be readily simulated even with seven overlapped broad powder patterns. The simulated spectrum shown in Fig. 3b is produced using the POWDER simulation program developed previously (*14*), where the influence of the slow sample turning is not considered. Seven sets of the tensor principal values corresponding to the seven different powder patterns were used for the simulation of the 2D CSA-CSA spectrum. A Gaussian line broadening of 8 ppm in both dimensions was applied. The simulation was initialized using the experimental principal values from the triple-echo MAT measurements (*3*) reported previously. During the simulation, the relative distance of the principal values for any one set of the principal values was locked and constrained such that each individual pattern could only move along the twofold symmetric axis of the spectrum during the simulation process. Because of the high intensity of the powder patterns for the methoxy

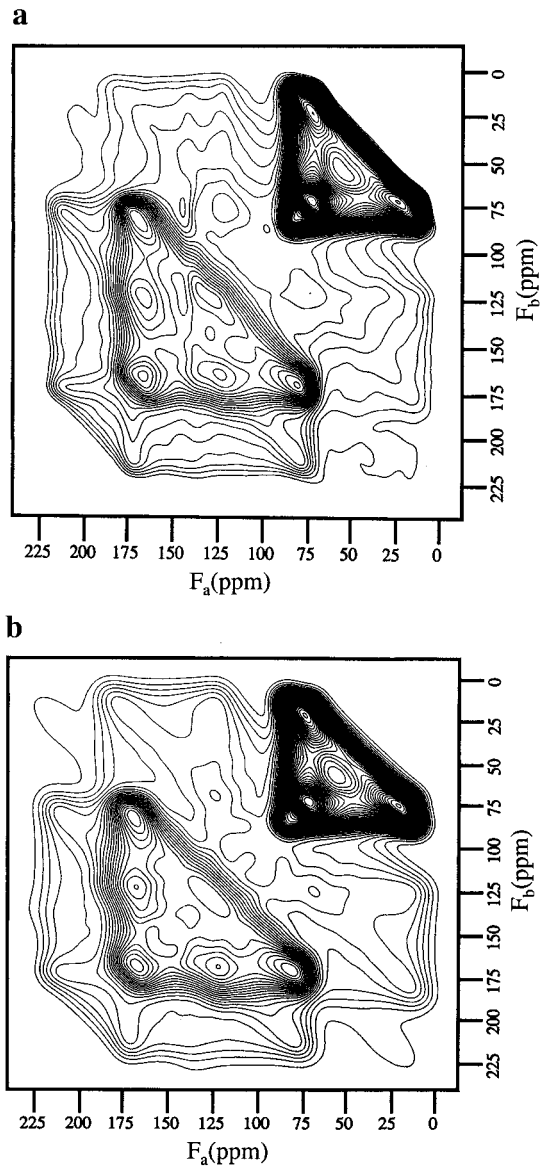

FIG. 3. (a) Contour plot of the experimental ^{13}C MAT 2D CSA-CSA correlation spectrum of 1,2,3-TMB. (b) Contour plot of the simulated 2D CSA-CSA correlation spectrum of 1,2,3-TMB. In both (a) and (b), the contour interval is 2% and the lowest contour plotted is 2% of the maximum peak height.

carbons, a small phase distortion in the OCH_3 powder patterns was found to interfere with the simulation of low-intensity CSA-CSA powder patterns. This distortion is especially noticeable in the pattern for C_5. In order to obtain a reasonable simulation, the principal values for the methoxy carbons were locked. The simulated final principal values for the different carbon produced deviations less than ± 2 ppm from the initial starting values. This general agreement between the triple-echo version of the MAT experiment and the current experiment is typical of most powder methods.

The results on 1,2,3-TMB from the MAT 3D CSA-CSA-CSA correlation experiment using the pulse sequence in Fig. 2b are summarized in Figs. 4 and 5. The experimental conditions were as follows: The contact time was 5 ms. The 90° pulse width for ^{13}C channel was 9.5 μs. The recycle delay time was 8 s. The sample spinning rate was 44 $\pm$ 0.2 Hz. $\Delta = 50$ μs. The spectral widths $sw_a = sw_b = sw_c = 15{,}625$ Hz = 310.8 ppm, corresponding to a time domain increment of 64 μs for each individual dimension. The experimental data were collected in the following way. For each t_c increment, a 2D experiment consisting of 32 t_b and 256 t_a increments was acquired. The number of accumulations for each individual FID (i.e., a pair of fixed t_c and t_b values) was 16. Hence, the time needed to acquire one set of 2D data is $32 \times 16 \times 4 \times 8$ s, i.e., 4.55 h. A total of 32 sets of 2D data sets described by Eqs. [5–8] were acquired. Hence the total time required to acquire a 3D data set was 4.55×32, approximately 146 h. The spinning rate changed by less than ± 0.2 Hz during the experiment. The 3D data set was transferred to a data station where the 3D hypercomplex data were constructed according to Eqs. [9–11]. The time domain data in both t_b and t_c dimensions were zero filled to 256 points before Fourier transformation. After the Fourier transformation, the 3D spectrum may be improved by symmetrizing the data using the sixfold permutational symmetry inherent in the technique. This produces an increase in S/N by a factor of $6^{1/2}$.

In order to select a specific 2D powder pattern, all of the data are first projected onto the diagonal of the spectral cube. The resultant spectrum, shown in Fig. 4, resembles a high-quality MAS spectrum, from which the isotropic chemical shift position for each carbon can be determined. Since the CSA-CSA-CSA powder patterns for resolved isotropic chemical shift positions lie in planes perpendicular to the diagonal of the cubic spectrum (i.e., the isotropic shift planes), projection of the data in an isotropic chemical shift plane onto the F_a–F_b 2D

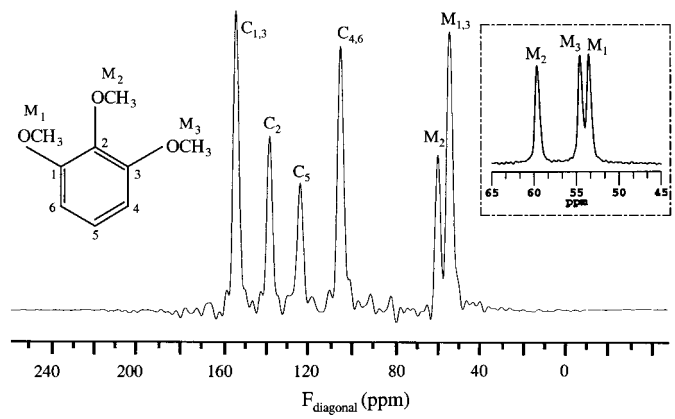

FIG. 4. The isotropic chemical shift projection of the MAT 3D CSA-CSA-CSA correlation spectrum of 1,2,3-TMB. Due to truncation of the FID in the 3D experiment, the resonances corresponding to the methoxy carbons (M_1 and M_3) are unresolved in this projection. The inset shows a conventional ^{13}C CP/MAS spectrum for the methoxy carbons acquired at a spinning rate of 6 kHz and at the same magnetic field strength.

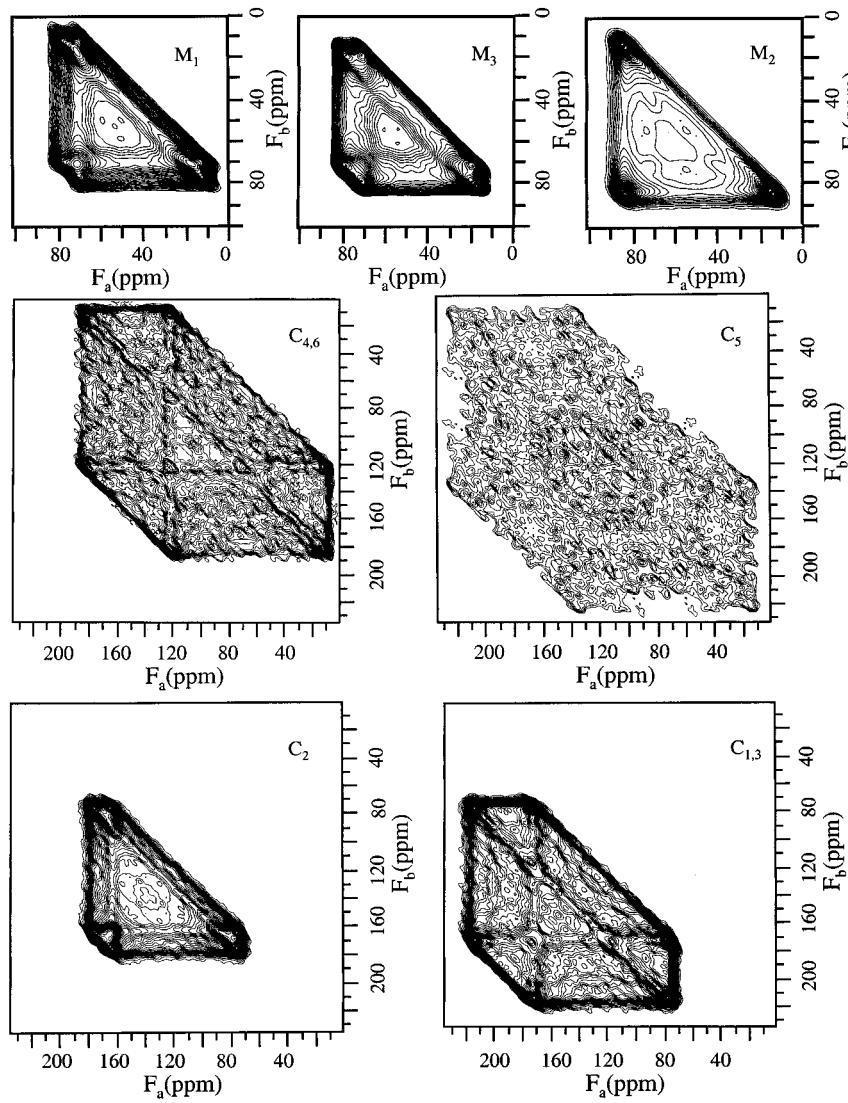

FIG. 5. The projection of the isolated MAT 3D CSA-CSA-CSA correlation spectrum of 1,2,3-TMB onto the F_a–F_b 2D spectral plane. Because of the diversity of tensors, a variety of plotting parameters must be used to provide optimal visualizations of the different carbons. These plotting parameters are given, respectively, for the contour interval and lowest contour in percentages of maximum peak height as follows: M_1 (3 and 8%), M_3 (3 and 12%), M_2 (2 and 5%), $C_{4,6}$ (1 and 6%), C_5 (1 and 4%), C_2 (2 and 8%), $C_{1,3}$ (1.5 and 6%).

spectral plane produces a 2D CSA-CSA powder pattern that resembles the conventional 90° sample reorientation spectrum. The resulting contour plots of this CSA-CSA powder pattern for each carbon in 1,2,3-TMB are illustrated in Fig. 5. Although the resonances for the methyls M_1 and M_3 are not completely resolved in the isotropic chemical shift projection in Fig. 4 due to the truncation of the FIDs, the 4-ppm difference between the two δ_{33} components is readily visualized by selecting 2D projections of the 3D spectral responses at various frequencies across the overlapped isotropic resonances.

The isolated single CSA-CSA powder patterns in Fig. 5 may be simulated in a straightforward way and principal values of the chemical shift tensors can thus be obtained (*14*). As in the case of the triple-echo MAT experiment (*3*), the best simulated principal values are in excellent agreement with those from the single crystal study (*22*). The differences between the simulated principal values and those from the single crystal study are found to be within ± 2 ppm.

The method presented in this work differs from the 3D slow-spinning version of the 3D DECODER experiment (*19*) in the following particulars. Three storage pulses were used in Ref. (*19*), while two are used in our approach. Since each storage pulse projects only a cosine or a sine component of the total magnetization, greater sensitivity is realized in the present experiment. The new approach correlates three orthogonal directions while in Ref. (*19*) only two orientations were correlated. The third dimension in the new approach may be useful for interpreting experimental results on orientationally

preferred samples. Rotor synchronization with preferred orientational directions is required. However, the method in Ref. (*19*) has the flexibility of correlating two spatial orientations with arbitrary angles other than the 90° used in Ref. (*14*) and in this work.

4. CONCLUSIONS

A 90° sample reorientation ^{13}C 2D CSA-CSA correlation spectrum can be produced by employing constant slow sample rotation about the magic angle axis and by synchronizing the read pulse to $\frac{1}{3}$ of the rotor cycle. A high-resolution 3D CSA-CSA-CSA correlation experiment based on the MAT technique is reported in which the overlapped conventional 90° 2D CSA-CSA powder pattern for each carbon in a system with a number of inequivalent carbons can be separated according to its isotropic chemical shift value. The technique is demonstrated on 1,2,3-trimethoxybenzene, where the conventional 90° 2D CSA-CSA powder pattern for each carbon is successfully obtained. The high-resolution 3D CSA-CSA-CSA technique is also promising for the investigation of oriented samples with complex molecular structures when the rotor position is synchronized with the orientationally preferred directions.

ACKNOWLEDGMENTS

The authors acknowledge Dr. D. W. Alderman for the specific computer software used in processing the experimental data and also for his many valuable suggestions. This work was supported by the Office of Basic Energy Science of DOE under Grant DE FG02-94 ER 14452, by the NIH under GM 08521-37, and by Pittsburgh Technology Center by a contract to the Consortium for Fossil Fuel Liquification Science.

REFERENCES

1. Z. Gan, *J. Am. Chem. Soc.* **114,** 8307 (1992).
2. (a) J. Z. Hu, D. W. Alderman, C. Ye, R. J. Pugmire, and D. M. Grant, *J. Magn. Reson. A* **105,** 82 (1993); (b) Z. Gan, *J. Magn. Reson. A* **109,** 253 (1994).
3. J. Z. Hu, A. M. Orendt, D. W. Alderman, R. J. Pugmire, C. Ye, and D. M. Grant, *Solid State NMR* **3,** 181 (1994).
4. J. Z. Hu, W. Wang, F. Liu, M. S. Solum, D. W. Alderman, R. J. Pugmire, and D. M. Grant, *J. Magn. Reson. A* **113,** 210 (1995).
5. Z. Gan and R. R. Ernst, *J. Magn. Reson. A* **123,** 140 (1996).
6. (a) D. W. Alderman, G. McGeorge., J. Z. Hu, R. J. Pugmire, and D. M. Grant, *Mol. Phys.* **95**(6), 1113 (1998); (b) G. McGeorge, J. Z. Hu, C. L. Mayne, D. W. Alderman, R. J. Pugmire, and D. M. Grant, *J. Magn. Reson.* **129,** 134 (1997); (c) G. McGeorge, D. W. Alderman, and D. M. Grant, *J. Magn. Reson.* **137,** 138 (1999).
7. E. Hughes, E. B. Brouwer, and R. K. Harris, *J. Magn. Reson.* **138,** 256 (1999).
8. (a) A. Philippou, F. Salehirad, D. P. Luigi, and M. W. Anderson, *J. Chem. Soc. Faraday Trans.* **94,** 2851 (1998); (b) A. Philippou, F. Salehirad, D. P. Luigi, and M. W. Anderson, *J. Phys. Chem. B* **102,** 8974 (1998).
9. (a) J. Z. Hu, M. S. Solum, R. J. Pugmire, C. Ye, and D. M. Grant., *Energy Fuels* **9,** 717 (1995); (b) J. C. Facelli, J. Z. Hu, A. M. Orendt, A. M. Arif, R. J. Pugmire, and D. M. Grant, *J. Phys. Chem.* **98,** 12186 (1994); (c) W. Wang, J. Z. Hu, D. W. Alderman, R. J. Pugmire, and D. M. Grant, *Solid State NMR* **5,** 257 (1995); (d) W. Wang, C. G. Phung, D. W. Alderman, R. J. Pugmire, and D. M. Grant, *J. Am. Chem. Soc.* **117,** 11984 (1995); (e) J. K. Harper, G. McGeorge, and D. M. Grant, *J. Am. Chem. Soc.* **121,** 6488 (1999).
10. S. L. Gann, J. H. Baltisberger, and A. Pines, *Chem. Phys. Lett.* **210,** 405 (1993).
11. A. Bax, N. M. Szeverenyi, and G. E. Maciel, *J. Magn. Reson.* **52,** 147 (1983).
12. J. Z. Hu, A. M. Orendt, D. W. Alderman, C. Ye, R. J. Pugmire, and D. M. Grant, *Solid State NMR* **2,** 235 (1993).
13. (a) A. Ramamoorthy, L. M. Gierasch, and S. J. Opella, *J. Magn. Reson. B* **110,** 102 (1996); (b) J. Z. Hu, D. W. Alderman, R. J. Pugmire, and D. M. Grant, *J. Magn. Reson.* **126,** 120 (1997).
14. (a) C. D. Hughes, Ph.D Dissertation, Department of Chemistry, University of Utah (1991); (b) C. D. Hughes, M. H. Sherwood, D. W. Alderman, and D. M. Grant, *J. Magn. Reson. A* **102,** 58 (1993).
15. M. L. Hsu, D. M. Grant, R. J. Pugmire, Y. Korai, S. H. Yoon, and I. Mochida, *Carbon* **34**(6), 729 (1996).
16. K. Schmidt-Rohr, M. Hehn, D. Schaefer, and H. W. Spiess, *J. Chem. Phys.* **97,** 2247 (1992).
17. B. F. Chmelka, K. Schmidt-Rohr, and H. W. Spiess, *Macromolecules* **26**(9), 2282 (1993).
18. P. M. Henrichs, *Macromolecules* **20,** 2099 (1987).
19. R. H. Lewis, H. W. Long, K. Schmidt-Rohr, and H. W. Spiess, *J. Magn. Reson. A* **115,** 26 (1995).
20. D. J. States, R. A. Haberkorn, and D. J. Ruben, *J. Magn. Reson.* **48,** 286 (1982).
21. E. A. Hill and J. P. Yesinowski, *J. Chem. Phys.* **106,** 8650 (1997).
22. C. M. Carter, J. C. Facelli, D. W. Alderman, D. M. Grant, N. K. Dalley, and B. E. Wilson, *J. Chem. Soc., Faraday Trans. 1* **84**(11), 3673 (1988).